

Robustness of Shor's algorithm with implications to scaling and quantum error correction.

Simon J. Devitt, Austin G. Fowler and Lloyd C. L. Hollenberg.

Centre for Quantum Computer Technology, School of Physics

University of Melbourne, Victoria 3010, Australia.

(Dated: February 20, 2019)

Shor's algorithm is a combination of both classical pre and post-processing and a quantum period finding subroutine (QPF) which allows for the exponential speed up of this algorithm on a quantum device. We consider the stability of this subroutine when exposed to a discrete error model that acts to perturb the computational trajectory of a quantum computer. Through detailed state vector simulations of an appropriate quantum circuit, we show that the structure of the circuit itself heavily influences the probability of success of the QPF subroutine. The naive estimate on component precision, based on the total number of possible error locations is shown to be too conservative and we find evidence for a polynomial scaling in the number of tolerable errors as a function of problem size. The results of these simulations are then used to examine the most appropriate use of quantum error correcting (QEC) codes for both the practical problem of factoring and the testing of a large scale quantum algorithm on prototype quantum computers.

The investigation and implementation of large scale quantum algorithms is arguably of enormous importance to the field of quantum information and computation. The seminal work by Shor in 1994 [2] was the first example of a complex and large scale algorithm that was able to efficiently solve a classically intractable problem and hence is a prototype example for all complex quantum codes.

Since Shor's discovery, the construction of a large scale quantum computer (QC) has been an area of intense research. Currently there are many different proposals for constructing such a device [8, 9], but despite significant progress the issue of decoherence and imperfect gate design begs the question of whether such a large and complex algorithm can be experimentally realized beyond trivial problem sizes.

The development of quantum error correction (QEC) [10] and fault-tolerant quantum computation [8] has shown theoretically how large scale algorithms can be implemented on imperfect devices. However, without a working QC, detailed classical simulations of QEC and quantum algorithms constitute the only method for reliable information regarding the behavior of such schemes and the ease in which they can be implemented on physical systems. The issue of appropriate use of QEC and the construction of arbitrary fault-tolerant gates [26] still requires detailed knowledge of the behavior of the underlying algorithm in order to tailor these schemes appropriately.

For large scale quantum algorithms, the general method of analysis is to assume that all components within the algorithm have a precision of $1=n_p$, where $n_p = KQ$ represents the number of locations where an error can occur during an operation utilizing Q qubits and K elementary steps (depth of the circuit). For small quantum circuits, this approximation is not an obstacle in component design. However, for more complex codes, where qubits may be coupled in highly non-trivial ways, it is not obvious that such naive considerations to circuit analysis are sufficient. In fact our results show that they are not. In this analysis we examine the quantum period finding (QPF) subroutine due to its importance to the field of

quantum computing and because it is a good example of a well known, non-trivial algorithm.

Circuits to factor large integers, for example a 128-bit number requires n_p to be of the order $10^7 - 10^{10}$ depending on the specific circuit used. Engineering components of this precision is currently far from being experimentally realized in any of the numerous architectures currently proposed. Our analysis of circuit stability based on explicit simulations, shows that the $1=n_p$ bound for component precision for these complex circuits is not absolute. We find evidence for an additional polynomial scaling in component precision, $P(L)=n_p$, with $P(L)$ at least linear. This additional scaling has major implications when testing such complex codes on prototype quantum computers.

The development of QEC has undoubtedly been the catalyst to the development of quantum computers. Without QEC it is commonly accepted that such large scale quantum algorithms would be impossible due to decoherence and imperfect quantum gates. However, there has yet to be any detailed work into the effective implementation of known QEC codes and what may be the most appropriate use of such codes for known algorithms such as Shor's QPF subroutine. Based on the work of Steane [6], we provide a simple analysis of what may be the most effective QEC codes to implement when testing the QPF subroutine on a prototype device and when attempting to factor a specific L bit number.

Several authors have previously examined the effects of errors on Shor's algorithm [12, 13, 19]. These simulations are often limited to specific sections of the entire circuit, or to other sources of error such as phase drifts on idle qubits, imperfect gate operations or aspects relating to quantum chaos. Chuang et al [4] was one of the first to look at the error stability of Shor's algorithm, analytically, under the effects of environmental coupling. Miquel et al [5] examined the stability of Shor's algorithm using an identical error model to that used in this investigation. However, the stability of the algorithm was only investigated for a single problem size and did not investigate how the stability changes as the

problem size increases.

Most circuit designs for the QPF subroutine assume that arbitrary qubits can be coupled directly (non-LNN). However, several architectures, most notably solid state models are restricted to a single line of qubits with nearest neighbor interactions only (LNN). The issue of whether the QPF subroutine can be implemented on such LNN architectures is also investigated, with results indicating that if LNN circuits can be designed with comparable values for n_p , then the stability of such circuits under errors is equivalent.

The following will examine specific circuits for both LNN and non-LNN architectures in the presence of a discrete error model, in order to determine:

1. The degree to which the final required state of the computer is effected by small changes in the computational trajectory caused by these errors.
2. The impact of a LNN architecture on the reliability of the QPF subroutine.
3. If the $1=n_p$ bound for component precision remains absolute for various problem sizes.

This paper is organized as follows. Section I examines the underlying theory behind Shor's algorithm, the QPF subroutine and how success is defined. Section II details the error model and issues relating to simulations. Section III present simulation results examining the stability of the QPF subroutine near the $1=n_p$ lower bound for both LNN and non-LNN circuits. Finally, section IV looks to the demands on QEC and concatenated codes. Specifically, examining the most appropriate use of multiple QEC codes to tailor the resource requirements to specific problem sizes.

I. SHOR'S ALGORITHM

As several papers detail the major steps of Shor's algorithm [2, 14, 15], we provide an overview for the sake of completeness and to introduce notation. We first consider a given composite number $N = N_1 N_2$ which has a binary length $L = \log_2(N)$. To factorise this number, we consider the function $f(k) = x^k \bmod N$, where $k \in \mathbb{Z}$ and x is a randomly chosen integer such that $1 < x < N$ and $\gcd(N; x) = 1$ (\gcd greatest common divisor). The QPF subroutine of Shor's algorithm determines the period of $f(k)$. i.e. to find the integer $r > 0$ such that $f(r) = 1$. This QPF subroutine is the quantum component of Shor's algorithm. The complete algorithm is composed of both the QPF subroutine and several pre and post processing operations that can be performed in polynomial time using classical techniques. These classical steps are detailed by several authors [2, 8, 15], for our purposes we assume that these classical steps can be implemented in polynomial time with no error. Once the QPF subroutine returns a value for the period of $f(k)$ the factors

of N can be calculated as $N_1 = \gcd(f(r=2) - 1; N)$ and $N_2 = \gcd(f(r=2) + 1; N)$, conditional on r being even and $f(r=2) \notin N - 1$.

In general, to factorise a number of binary length L first requires the initialization of $3L$ qubits to the state $|j_{2L} j_{1L} \rangle$. For clarity we have broken these $3L$ qubits into $2L$ qubits to store the values k and L qubits to store the function evaluations $x^k \bmod N$. A Hadamard transform is performed on each of the $2L$ qubits,

$$|j_{2L} j_{1L} \rangle \xrightarrow{H} \frac{1}{2^L} \sum_{k=0}^{2^L-1} |k_{2L} k_{1L} \rangle : \quad (1)$$

Step three is to apply the function $f(k)$ on the L qubit register, conditional on the values k in the $2L$ qubit register. The resultant state of the computer is,

$$\frac{1}{2^L} \sum_{k=0}^{2^L-1} |k_{2L} k_{1L} \rangle \xrightarrow{f(k)} \frac{1}{2^L} \sum_{k=0}^{2^L-1} |k_{2L} k^k \bmod N \rangle : \quad (2)$$

The next step is to measure the L qubit register,

$$\frac{1}{2^L} \sum_{k=0}^{2^L-1} |k_{2L} k \rangle \xrightarrow{M_L} \frac{p}{2^L} \sum_{n=0}^{2^L-1} |n_{2L} n \rangle : \quad (3)$$

Where r is the period of f , f_0 is the measured value and k_0 is the smallest value of k such that $f_0 = f(k_0)$. We now apply a quantum Fourier transform (QFT) to the k register. The state of the computer after the application of the QFT becomes,

$$\frac{p}{2^L} \sum_{j=0}^{2^L-1} |j_{2L} j_{1L} \rangle \xrightarrow{QFT} \frac{p}{2^L} \sum_{n=0}^{2^L-1} \exp \left(\frac{2\pi i}{2^L} j(k_0 + nr) \right) |j_{2L} j_0 \rangle : \quad (4)$$

If we now measure the k register, we will return a value of j with probability,

$$p(j; r; L) = \frac{p}{2^L} \sum_{n=0}^{2^L-1} \exp \left(\frac{2\pi i}{2^L} jnr \right)^2 : \quad (5)$$

Equ. 5 is strongly peaked at certain values of j . If the period r perfectly divides 2^L then equ. 5 can be evaluated exactly, with the probability of observing $j = c2^L = r$ for $0 < c < r$ being $1=r$, and 0 if $j \notin c2^L = r$ [Fig. 1(a)]. If r is not a perfect divisor of 2^L , then the peaks of equ. 5 become slightly broader, [Fig. 1(b)]. In this case, classical methods can be utilized in order to determine r from the measured values of j . Given several measured integer values around these non-integer peaks a continued fractions method can be employed to determine r [8, 15]. The probability of success s for Shor's algorithm is generally defined as,

$$s(L; r) = \sum_{j \in \text{useful } jg} p(j; L; r); \quad (6)$$

where $\text{useful } jg$ is the set, $j = bc2^L = rc$, $j = dc2^L = re$, $0 < c < r$, where $b \leq d \leq e$ denote rounding down and up

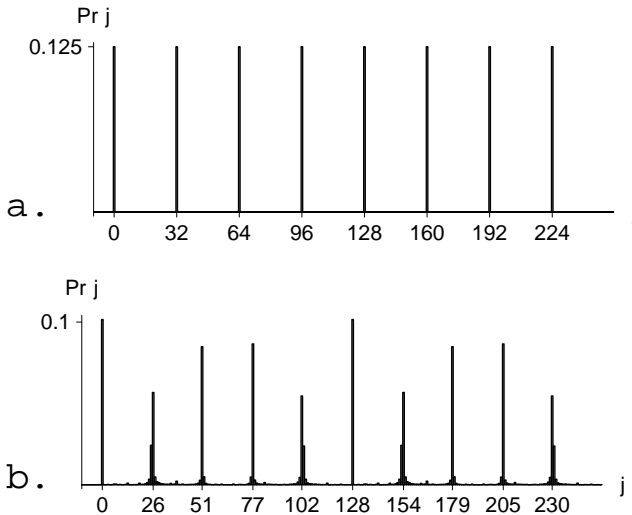


FIG. 1: Plot of equ. 5 for the case, $2^{2L} = 256$ with a) $r = 8$ and b) $r = 10$.

respectively and $p(j; L; r)$ is defined via equ. 5. Using this definition of s we determine the period r after $O(1=s)$ calls to the subroutine.

Many circuits have been proposed in order to implement the QPF subroutine on a physical quantum computer, as summarized in table I. Some are optimized for conceptual

Circuit	Qubits	Depth
Simplicity [16]	$5L$	$O(L^3)$
Speed [17]	$O(L^2)$	$O(L \log L)$
Qubits [18]	$2L$	$32L^3$
Tradeoff 1 [20]	$50L$	$2^{19}L^{1.2}$
Tradeoff 2 [20]	$5L$	$3000L^2$

TABLE I: Number of qubits required and circuit depth of different implementations of the QPF subroutine. Where possible, figures are accurate to leading order in L .

simplicity [16], some for speed [17] and some for utilizing a minimum number of qubits [18].

This investigation will focus on circuits that require a minimal number of qubits for two reasons. Entanglement is a powerful resource available to quantum computers that cannot be efficiently simulated on classical computers. Hence, minimizing the total number of qubits and the total amount of entanglement is a necessary requirement for faster simulations. Also, in the short term, many current QC architectures face a difficult hurdle in fabricating a large number of reliable qubits, making minimal qubit circuits desirable.

Beauregard [18] details an implementation of the QPF subroutine appropriate for architectures allowing for the arbitrary coupling of qubits (non-LNN) in which modular addition and multiplication circuits are performed in Fourier space. An appropriate circuit for Linear Nearest Neighbor

(LNN) architectures used in this investigation detailed in ref. [21] uses the same method in order to reduce the total number of qubits required. Both the LNN circuit and a slightly modified version of the Beauregard circuit requires $2L + 4$ qubits and have identical depths and gate counts to leading order in L .

II. ERROR MODELS AND ANALYSIS

In our simulations, errors were simulated using the discrete model in which a single qubit j $i = j_i + j_{li}$ can experience a bit flip $X j_i = j_i + j_{li}$, a phase flip $Z j_i = j_i - j_{li}$ or both at the same time $X Z j_i = j_i - j_{li}$. These operators are the set $\{X, Z, Y\}$.

These discrete error operators are then applied to each qubit, after each operational time step with probability $p=3$ (i.e each error has identical probability of occurrence, with the total probability of error given by p). The operational time for all two qubit gates are assumed to be identical and all single qubit gates combined with neighboring two qubit gates via the canonical decomposition [22, 23, 24]. The discrete error model represent the most common error model used within QEC analysis. This model oversimplifies error effects within a quantum computer in several ways.

1. The error model used is uncorrelated and random. Some architectures may be more vulnerable to dephasing errors (Z operations), relaxation errors (X operations) or loss of qubits (this is particularly relevant in linear optical systems [3]).
2. This model does not examine the effects of systematic errors due to such things as inaccurate gates caused by mischaracterization [27] of single and two qubit Hamiltonians or systematic rotation errors.
3. This specific error model treats memory errors and gate errors identically, which may not be realistic given a specific physical architecture.

Although this model represents a simplification of the many effects that can cause errors within a quantum computer, it represents a convenient framework for examining the stability of the computational state that exists during the QPF calculation. The effect of more specific error models depend heavily on the explicit QC architecture used.

We now describe the behavior of the QPF subroutine in the presence of severe errors. Referring to the quantum circuit used [21], j is obtained bit-by-bit via a series of sequential measurements on a master control qubit. This master qubit simulates the entire $2L$ qubit register described in section (I). The QFT on this single qubit required by equ. 4 is performed through a series of Hadamard gates and classically controlled single qubit rotations. In a more general analysis we can

model the entire computer as two registers, a single master qubit and the rest of the computer.

Consider the state of the computer at a point just before the application of a controlled modular multiplication gate. At this point the master control qubit is in an equal superposition of $\lvert \text{p}_i \rangle$ and $\lvert \text{j}_i \rangle$ and the rest of the computer is some unknown superposition,

$$\lvert \text{j}_i \rangle = \frac{1}{\sqrt{2}} (\lvert \text{p}_i \rangle_{\text{master}} + \lvert \text{j}_i \rangle_{\text{master}}) \quad \lvert \text{j}_i \rangle_{\text{computer}} : \quad (7)$$

Now apply the modular multiplication gate, which will return a new superposition state for the $\lvert \text{j}_i \rangle_{\text{computer}}$ register (when the master qubit is in the $\lvert \text{j}_i \rangle$ state). This new superposition is denoted through the coefficients, $f_{j,g}$,

$$\lvert \text{j}_i \rangle = \frac{1}{\sqrt{2}} \sum_{j=0}^{2^L-1} \lvert \text{p}_i \rangle + \frac{1}{\sqrt{2}} \sum_{j=0}^{2^L-1} \lvert \text{j}_i \rangle : \quad (8)$$

Prior to measurement, a classically controlled rotation (θ) and a second Hadamard gate is applied to the master control qubit. The value of θ is dependent on the result of all previous measurements on this qubit. Hence the state just before measurement is,

$$\begin{aligned} \lvert \text{j}_i \rangle &= \frac{1}{2} \sum_{j=0}^{2^L-1} \lvert \text{p}_i \rangle \left(e^{i\theta_j} \lvert \text{j}_i \rangle \right) \\ &+ \frac{1}{2} \sum_{j=0}^{2^L-1} \lvert \text{j}_i \rangle \left(e^{i\theta_j} \lvert \text{j}_i \rangle \right) : \end{aligned} \quad (9)$$

With the probability of measuring a 1 or 0 is given by,

$$p\left(\frac{1}{2}, \frac{1}{2}\right) = \frac{1}{2} \left(\frac{1}{4} \sum_{j=0}^{2^L-1} (e^{i\theta_j} \lvert \text{j}_i \rangle \lvert \text{j}_i \rangle + e^{-i\theta_j} \lvert \text{j}_i \rangle \lvert \text{j}_i \rangle) \right); \quad (10)$$

using,

$$\sum_{j=0}^{2^L-1} \lvert \text{j}_i \rangle \lvert \text{j}_i \rangle = \sum_{j=0}^{2^L-1} \lvert \text{j}_i \rangle \lvert \text{j}_i \rangle = 1: \quad (11)$$

Errors cause the summation in equ. 10 to asymptote to 0 resulting in an equal probability $p = 0.5^{2L}$ of each j being observed.

The period of the function r dictates the number of non-zero coefficients $f_{j,g}$ and the specific value of j simply changes the sequence of 1's and 0's measured at each step. Since errors act to randomly perturb these sets of coefficients, considering different values of r and/or j will have no effect on the stability of the QPF subroutine.

The simulated QPF circuit is extremely complex and hence requires a large amount of classical simulation time.

Ideally, simulations would proceed by applying a single discrete error gate to every possible location within the circuit and averaging the probability of success, s , over all possible locations. For example, fig. 2 shows the effect of a single \times error on the QPF success probability, s , for the first modular multiplication gate in the $L = 5$ circuit. From this we can see

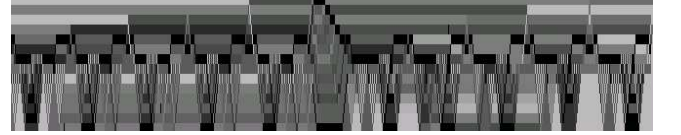


FIG. 2: Map showing how the location of a single bit flip error plays a major role in the final output success of the LNN circuit. This image is for $L = 5$ (14 qubits), and shows the first modular multiplication section of the circuit. Each horizontal block represents one of the 14 qubits while each vertical slice represents a single time step. Darker areas represent successively lower values for s .

that the spatio-temporal location of an error plays a major role in the final value of s calculated, with various sections invariant to the bit flip error. In order to analyze the behavior of the QPF subroutine we take an ensemble average over all possible error locations. For example, in fig. 2, the average value of s over all possible locations for a single error is $s = 0.34$. Most circuits are far too large to map out this topology efficiently. Hence, we will take 50 statistical runs to obtain an approximate average value of s for these circuits.

III. STABILITY UNDER A FIXED NUMBER OF ERRORS

The classical simulation algorithm employed used a state vector representation. Matrix operations were performed to simulate both quantum gates and error operations. Figs 3 and 4 show the results for $2L + 4 = 14; 16; 18; 20$, representing factorization of composite numbers from $N = 27$ to $N = 247$. Simulations examined functions that each had a period $r = 6$. Table II show the functions $f(k)$ used for each value of L .

$2L + 4$	$f(k) = x^k \bmod N$, with $r = 6$
14	$8^k \bmod 27$
16	$31^k \bmod 63$
18	$10^k \bmod 77$
20	$27^k \bmod 247$

TABLE II: Functions used for various values of L . Note that for $2L + 4 = 14; 16$ the functions used are not products of two primes. With some slight modifications to the classical post-processing, Shor's algorithm can still be used to factor such numbers. Since we are only investigating the reliability of the QPF subroutine, this is not relevant to our analysis.

These simulations aim to investigate the behavior of the QPF subroutine for high component precision, close to the $1=n_p$ bound. Simulations were performed in a half-stochastic, half-deterministic manner: The type and

spacio-temporal location of discrete errors occur at random, however we specify exactly how many errors can occur within a given run of the subroutine.

Simulations examine the probability of obtaining the specific useful value $j = b2^{2L} = 6c$. Figs 3 and 4 show the results for the non-LNN [18] and LNN [21] circuits respectively.

non-LNN QPF subroutine under fixed number of errors for various values of L .

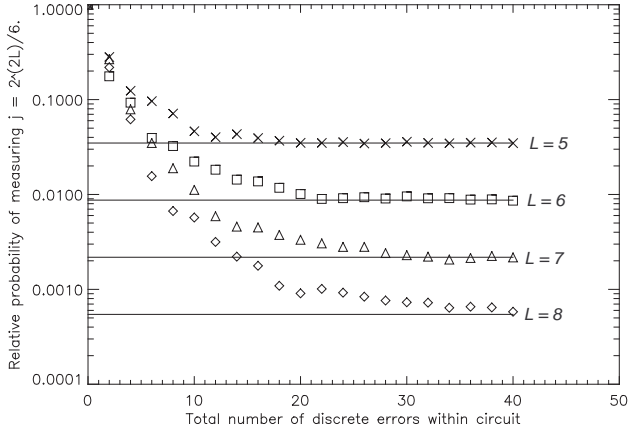


FIG. 3: Plot showing the relative probability of measuring $j = b2^{2L} = 6c$ as a function of the specific number of errors for the non-LNN circuit. The curves represent $L = 5$ to $L = 8$. The horizontal lines show the point of random output for each successive value of L .

LNN QPF subroutine under fixed number of errors for various values of L .

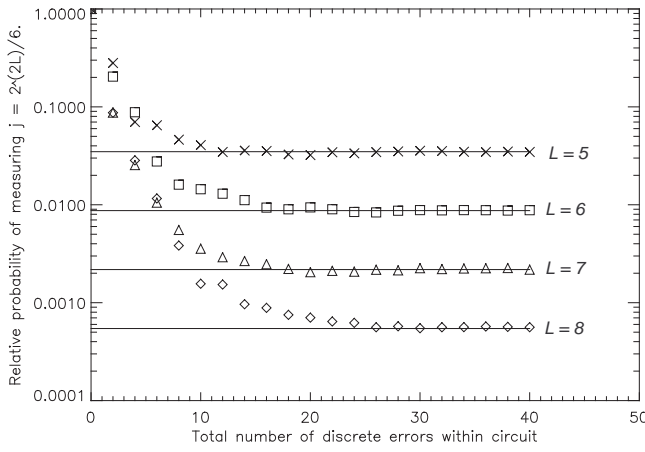


FIG. 4: Error stability for the LNN circuit. Equivalent to fig. 3

The definition of success for the QPF subroutine, given in section I takes into account that many different values of j may be used to determine r . However, for the sake of this analysis, we only care if the QPF subroutine returns with high probability a value of j that is theoretically predicted. Therefore in figs. 3 and 4 we normalize the plots such that an error free calculation returns $j = b2^{2L} = 6c$ with probability 1

and Shor's algorithm succeeds with a single call to the QPF subroutine. As the number of errors increase the probability of measuring $j = b2^{2L} = 6c$ decreases until it reaches the point of random output, at this stage the QPF subroutine performs no better than randomly choosing a value of j in the range $j = 0 ! j = 2^{2L}$.

Figs. 3 and 4 clearly shows how the quantum speed up of the QPF subroutine and hence Shor's algorithm diminishes to a point where it's no different to a classical search as the number of errors increases. Analytical expressions to these curves are extremely difficult to obtain from the limited amount of data available due to long computation times. Each point represents 50 separate simulations where the total number of errors occur randomly within the QPF circuits. In order to get sufficient data to extract meaningful analytical expressions for each of these curves, the number of statistical runs should be the same order as the number of possible error locations (or error combinations). For example, in the $L = 5$ circuit, for 1 error, the number of possible error locations and types is 18000. Hence, it is quite surprising that even 50 statistical runs provides enough data to obtain a qualitative picture of how the QPF subroutine behaves for various values of L .

The results of QPF simulations need to be examined from the standpoint of how much quantum speedup do we require for either practical implementation for Shor's algorithm, or testing complex codes on prototype quantum computers. For small L , the operational time of the QPF subroutine may allow for a large number of calls, enabling a probability spectrum of the register j to be plotted. If the probability spectrum contain peaks, then this would indicate the presence of quantum processing instead of a random selection from the j register. If the QPF subroutine is implemented for testing quantum codes, allowing multiple errors at the expense of multiple subroutine calls may be far simpler than introducing QEC protocols.

The practical implementation of the QPF subroutine for use as a factoring engine will generally not allow for multiple errors. Since the size of the j register increases as 2^{2L} , only a small number of calls to the QPF subroutine is desired for large L . Therefore, the use of QEC protocols to maintain a $1=n_p$ component precision for logical qubits is inevitable.

Regardless of the potential implementation of the QPF subroutine, either for testing or practical use, these simulations show that an absolute $1=n_p$ component precision for all problem sizes is not required to obtain better performance to a classical search. By inspection of figs 3 and 4, an estimate can be made regarding the number of errors (as a function of L) before the QPF subroutine performs no better than a classical search [Fig. 5]. Fig. 5 represents only a qualitative estimate from figs. 3 and 4 since the lack of statistical data makes the determination of analytical expressions to the curves impossible. However, in the authors opinion a polynomial scaling with L is likely. This implies that the maximum com-

ponent precision needed for the QPF subroutine scales not as $1=n_p$, but as $P(L)=n_p$ where $P(L)$ is at least linear, with the QPF subroutine still performing better than a classical search.

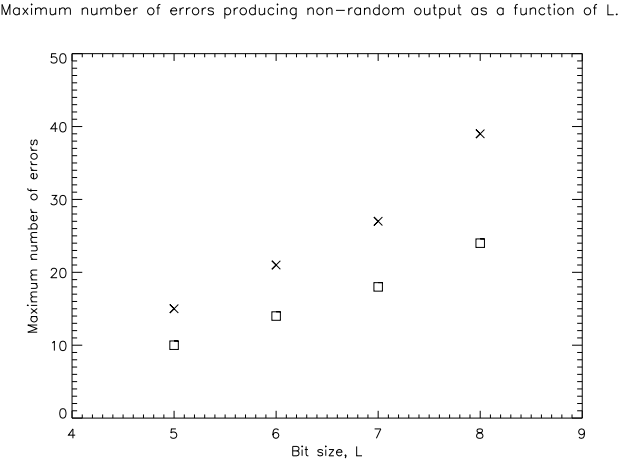


FIG. 5: Estimate on the maximum number of errors possible for each value of L before the LNN circuit becomes equivalent to a classical random search. (x) non-LNN circuit, (□) LNN circuit.

The error behavior for the LNN and non-LNN circuits are largely indistinguishable from each other. However, there is a slight difference in the error sensitivity of the two circuits. We attribute this to a minor increase in the LNN circuit depth. As expected, the overall area of the circuit is the dominating factor in its sensitivity. The mesh circuit [21] required in the LNN design is the major difference between the LNN and non-LNN circuits. This section of the LNN circuit acts to slightly increase the overall depth, from $32L^3 + 66L^2 - 2L - 1$ for the non-LNN circuit to $32L^3 + 80L^2 - 4L - 2$ for the LNN design [Table. III]. Hence the sensitivity of the LNN circuit increases slightly compared with the non-LNN circuit.

L	LNN Circuit	non-LNN Circuit
5	5978	5639
6	9766	9275
7	14866	14195
8	21470	20591

TABLE III: Total circuit depths for the LNN and non-LNN circuits, for $L = 5$ to $L = 8$

IV. IMPLICATIONS FOR QUANTUM ERROR CORRECTION

Quantum error correction (QEC) is commonly known to be a necessity for any realistic implementation of large scale and complex quantum algorithms. Currently there exists an extensive library of QEC codes based on error correction protocols used in classical computing. The most appropriate

use of this large collection of codes for specific quantum algorithms is still an important yet unanswered area of research.

Steane [6] has previously examined this issue from a different perspective. His work concentrated on 18 separate QEC codes (detailed in table IV) and examined the maximum circuit size (n_p) that can be implemented using these codes. We will take this analysis one step further. By using Steane's results and the previous QPF simulations, we will examine the resource requirements when attempting to factor integers of binary length up to $L = 10000$.

Our analysis is only applicable for non-LNN architectures due to issues relating to information transport for LNN error correction protocols. Three separate cases will be examined,

1. Single layer correction to factor large integers up to $L = 500$, assuming a physical component precision of 10^5 . For large factoring problems only a single QPF subroutine call is desired and hence *logical* component precision is bounded by $1=n_p$ [Fig. 6].
2. A multiple-layer concatenated correction scheme to factor very large integers (up to $L = 10000$) when physical component precision is decreased to 10^4 , looking at two separate types of concatenation. Two inner $[[7,1,3]]$ Hamming codes [Fig. 7] or a single inner $[[23,1,7]]$ Golay code [Fig. 8]. Again we assume *logical* component precision bounded by $1=n_p$.
3. Appropriate use of QEC when employing the QPF subroutine as a test algorithm for prototype devices [Fig. 9]. An ideal method for testing the QPF subroutine requires the generation of the probability spectrum for the register j , with non-classical behavior identified as peaks in this spectrum. The results of our simulations indicate that the effective component precision can now possibly scale at least as $L=n_p$. Hence less resource demanding codes (or no QEC) can be used, depending on L .

Since our analysis will be based heavily on Steane's prior work [6], table IV details the 18 separate QEC codes from [6] that we will compare. Included in the table are some useful parameters describing the code itself, including the number of physical qubits per logical block, n_p , the number of logical qubits encoded within each logical block, n_l , the number of error each code can correct, w , and the maximum weight of the check matrix w describing the code. w can be used to estimate the depth of any circuit used to prepare and verify ancilla qubits appropriate for the specific QEC code [7].

The results detailed in [6] determined the maximum circuit area n_p that can be implemented on a circuit encoded with each code before on average one uncorrectable error occurs.

Number	Code Name			d		w
0	None	1	1	1		
1	Hamming	7	1	3	1	3
2	Golay	23	1	7	3	11
3	Golay	21	3	5	2	7
4	BCH	31	11	5	2	15
5	QR	77	1	11	5	15
6	QR	45	3	9	4	15
7	QR	43	5	7	3	15
8	BCH	63	27	7	3	27
9	BCH	63	39	5	2	27
10	QR	79	1	15	7	27
11	QR	77	3	13	6	27
12	QR	75	5	11	5	27
13	QR	103	1	19	9	31
14	QR	101	3	17	8	31
15	QR	99	5	15	7	31
16	QR	97	7	13	6	31
17	BCH	127	29	15	7	47
18	BCH	127	43	13	6	47

TABLE IV: Properties of various QEC codes constructed from standard classical codes. Each code is specified by $[[n, k], d]$ where n is the number of physical qubits per logical block, k is the number of logical qubits per block and d is the distance of the code. n gives the number of errors that can be corrected by the code $n = (d - 1)/2$ and w gives the largest weight of a row or column used in the check matrix of the code. The code name is based on the classical code used to construct the applicable quantum code [28].

Fault-Tolerant error correction for each code requires a certain amount of ancilla preparation, verification, repeated syndrome measurement and correction for both X and Z errors. Hence implementing each code not only requires additional qubits but also additional time. Ref. [7] details a general method for preparing and verifying ancilla qubits for these codes, based on the relevant value of w .

Ancilla preparation for each code requires w time steps, while ancilla verification requires $w + 1 + T_m$ time steps, where T_m is the required time for a measurement. Our simulations assumed $T_m = 1$ (i.e. measurement gates require the same amount of time as a two-qubit interaction). The simulations in [6] specify $T_m = 25$ for all 18 codes. Our analysis also treat memory and gate errors equally, in contrast to [6]. However, since we are performing a comparative analysis between codes, these issues will not affect the qualitative nature of our conclusions.

Figs. 6,9,7 and 8 examines the qubit/time resources for each of the 18 codes in table IV for various values of L . The Y axis is simply the product $K^0 Q^0 10^7$, where K^0 and Q^0 now represent the total number of qubits and circuit depths needed for not only the algorithm, but for the overlaying correction protocol. The factor of 10^7 can be viewed as assuming gate operational times of 100ns.

The total number of qubits required when using each

code is given in [6] to be,

$$N = [+ \text{rep}(3 +)](2L + 4 + 10) = : \quad (12)$$

Where, rep is the number of ancilla states prepared in parallel for each correction stage taken to be = 1. and are specified via table (IV). The extra factor of 10 added to the number of actual qubits needed for the algorithm are workspace qubits needed for fault-tolerant gate operations. Generally this factor is less than 10 but we will be pessimistic.

The time taken for each round of QEC is given by $m(2w + 4)$, where $(2w + 4)$ is the number of time-steps required to measure an error syndrome and m represents the optimal number of syndrome measurements for each code (see table (I) in [6]). For each syndrome measurement, $w + w + 1 + T_m$ time steps are required to prepare and verify appropriate ancilla qubits (Here we assume $T_m = 1$). The coupling of ancilla qubits to the data block is assumed to take a single time step and the measurement of the ancilla block to determine the syndrome is also assumed to take a single time step.

The QPF circuit used has a un-encoded depth of $32L^3$, hence with QEC the total depth is assumed to be $K^0 32L^3 [m(2w + 4)]$. This value of K^0 assumes that a round of QEC is performed after each logical gate operation and that each logical gate operation required by the QPF circuit can be performed transversally and hence constitutes a single time step.

These assumptions in circuit design and operation are consistent with [6]. We also assume that the only difference in efficient circuit design between codes come from the number of required syndrome measurements, m , and the maximum weight of the check matrix, w , (which determines the number of total time steps needed for preparation and verification of ancilla blocks). Such issues as the required time to coupling ancilla qubits to the data block and the practical implementation of any of the required circuits for each code we assume to be identical for all codes and hence do not effect the final comparison. In reality these simplifying assumptions are unlikely to be valid (especially for appropriate LNN circuits). Further work will be required to adequately address these issues.

Fig. 6 examines the combined qubit/time resources required to factor numbers from $L = 5$ to $L = 500$ for no QEC and for each of the 18 codes specified in table IV, using a physical component precision of 10^{-5} . Fig. 6 assumes that we are attempting to practically implement the QPF subroutine to factor integers up to $L = 500$. Hence, we wish the QPF subroutine to return a j value expected through equ. 6 with only a single query. We expect that on average, no errors occur during calculation, this implies that each logical component must have precision of order $1 = n_p = 1 = (64L^4)$.

All points present in fig. 6 represent QEC codes that according to [6] are able to be implemented using circuits of

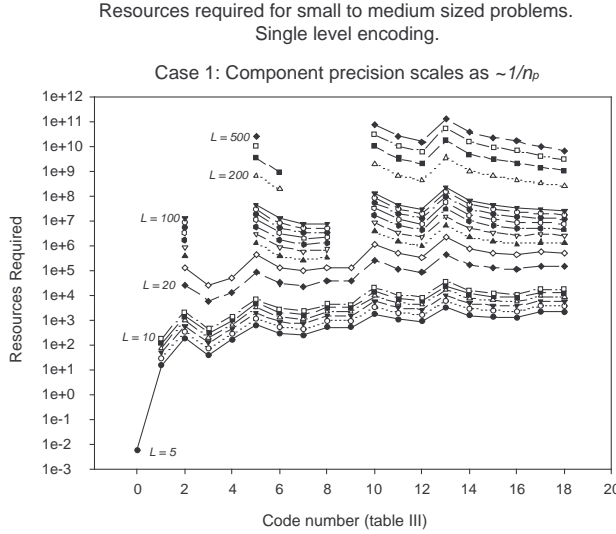


FIG. 6: Plot showing the resources needed $K^0 Q^0$ for factoring an L -bit number for no QEC or for each of the 18 codes in table (IV).

size $n_p > 64L^4$ before at least one uncorrectable error occurs. The number of uncorrected errors remaining in the encoded circuit will dictate if the QPF subroutine still performs better than a classical search. However, for large problem sizes shows in fig. 6 we assume that the QPF subroutine performs *ideally*, i.e. requires a single query. Table (V) summarizes the most appropriate code for each value of L .

bit-size (L)	Appropriate Code	Total Number of Qubits	Total circuit time (10^{-7})
5	None	14	0.0004
6	$[[7,1,3]]$ Hamming	754	0.0207
7	$[[7,1,3]]$ Hamming	812	0.0329
8	$[[7,1,3]]$ Hamming	870	0.0492
9	$[[7,1,3]]$ Hamming	928	0.0670
10	$[[7,1,3]]$ Hamming	986	0.0960
20	$[[21,3,5]]$ Golay	1848	3.48
30	$[[21,3,5]]$ Golay	2088	11.8
40	$[[43,5,7]]$ QR	4690	27.9
50	$[[43,5,7]]$ QR	5390	54.4
60	$[[43,5,7]]$ QR	6090	94.0
70	$[[43,5,7]]$ QR	6790	149
80	$[[63,27,7]]$ BCH	4340	380
90	$[[63,27,7]]$ BCH	4540	541
100	$[[63,27,7]]$ BCH	4740	742
200	$[[45,3,9]]$ QR	26474	3482
300	$[[45,3,9]]$ QR	38674	11750
400	$[[127,43,13]]$ BCH	14808	10352
500	$[[127,43,13]]$ BCH	17208	196000

TABLE V: Table showing for various values of L the most resource efficient code. Also shown is the number of qubits required [Equ. 12] and the total time needed for the circuit = $32L^3 \ln(2w + 4) \cdot 10^{-7}$

Appropriate QEC codes depend quite heavily on L . Steane's results concludes that for large algorithms the $[[127,43,13]]$

BCH code is the most appropriate in terms of the maximum n_p achieved and scale up. While this is true, if a quantum device is to be built to factor a specific L bit number, the actual code used should be chosen to minimize the resources needed.

For large quantum circuits, a single layer of QEC is sufficient for large L , provided experimental component precision can reach 10^5 . However, if we assume a more conservative value for component precision, concatenated error correction is required. Current experimental designs are attempting for component precision upper bound of 10^4 . This target was initially motivated by the first calculated thresholds for concatenated error correction [8].

Concatenated correction involves layering several QEC codes on top of each other. If one layer of QEC allows for a reduction in the failure of each level-1 encoded qubit, then by encoding several layer-1 qubits into a level-2 logical qubit failure rates of these level-2 qubits can be reduced even further [8]. If we reduce the component precision to this new value then unfortunately many circuits required to factor numbers with very large L become too large for a single level of error correction.

As well as the analysis into single level QEC encoding, [6] also examined the failure rate of circuits encoded with multiple layers of concatenated correction using the codes shown in table (IV). Once again we will use these results to examine the resources required to factor very large numbers, $L > 200$. Since we are looking at circuits to factor very large numbers, again a single query to the QPF is desired. We will consider two separate concatenations for factoring large L .

1. Concatenating each of the 18 codes with two inner $[[7,1,3]]$ Hamming codes.
2. Concatenating each of the 18 codes with a single inner $[[23,1,7]]$ Golay code.

As with the previous section, we will look at the resources required ($K^0 Q^0$) for each type of concatenation that can achieve the required precision for a given value of L .

Fig. 7 examines the product $K^0 Q^0 \cdot 10^{-7}$ using a single $[[23,1,7]]$ inner code concatenated with each of the 18 codes specified in table (IV). For each code $L = 200$ to $L = 10000$ is examined. Fig. 8 is an identical plot but using two inner $[[7,1,3]]$ Hamming codes concatenated with each of the 18 outer codes. Calculating the total number of qubits Q^0 and the total number of time-steps K^0 was done using a number of simplifying assumptions. However, since we are only attempting to compare the resources required between different codes this will not have a significant impact.

The total number of qubits for a single layer of correction was given by equ. 12. If we now consider the case where two inner $[[7,1,3]]$ Hamming codes are used, then the total

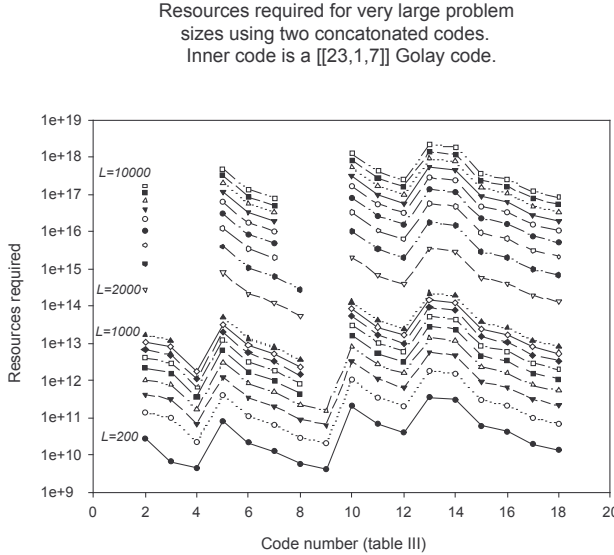


FIG. 7: Plot showing the resources needed for factoring large L -bit numbers using concatenated correction. This plot uses an inner [[23,1,7]] Golay code concatenated with each of the 18 codes shown in table (IV). Any combination of codes that cannot achieve the $1=n_p$ logical precision needed for a particular value of L are omitted from the plot.

number of qubits is given by,

$$N = \frac{1}{2} [n_2 + (3n_2 + n_2)] \\ [10n_2 + \frac{1}{1} [n_1 + (3n_1 + n_1)]] \quad (13) \\ [10n_1 + \frac{1}{0} [n_0 + (3n_0 + n_0)](2L + 4 + 10n_0)]:$$

$n_0 = n_1 = 7$ and $n_0 = n_1 = 1$ are for each of the two inner layers of Hamming codes. n_2 and n_1 are the associated values for the upper layer of correction for each of the 18 codes [table (IV)]. Each layer of correction has an additional fixed number of qubits = $10k_i$ as Fault-Tolerant workspace. The number of qubits for an inner layer [[23,1,7]] Golay code was calculated in a similar manner.

The number of time steps required for calculation was simplified using the following assumptions,

1. Error correction for multiple layers have to be performed sequentially. i.e. level-1 correction cannot proceed while level-2 correction is in progress.
2. All logical operations for each layer of encoding are transversal. i.e if an operation takes b time steps on un-encoded qubits then it takes b time steps for any level logical qubit.
4. All classical processing involved in QEC is much quicker than quantum operations and are independent of the

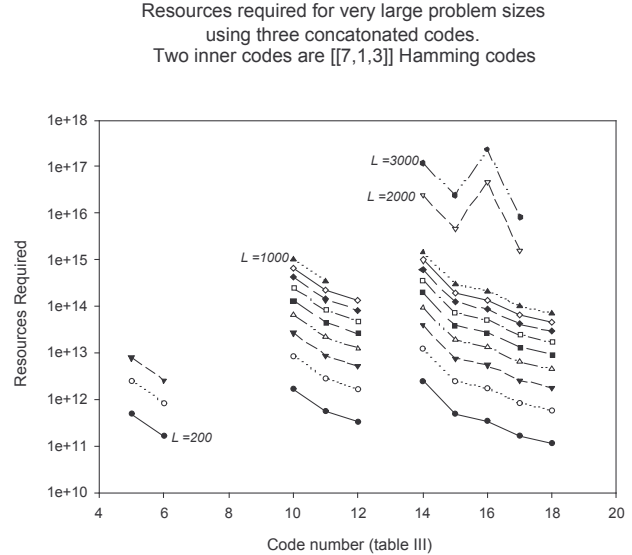


FIG. 8: Plot showing the resources needed for factoring large L -bit numbers using concatenated correction. This plot uses two inner [[7,1,3]] Hamming codes concatenated with each of the 18 codes shown in table (IV). A large number of code combinations using this type of concatenation cannot achieve the $1=n_p$ logical precision needed for larger values of L and are omitted from the plot.

level of encoding.

5. If the highest level of encoding requires a correction after each logical gate operation, then the next level down requires correction after every second logical gate operation, the next level down after every fourth gate operation, etc.

Assumptions 2,4 and 5 substantially simplify any actual realization of concatenated correction circuits. Provided that the increased complexities removed by these assumptions are common to all codes then these assumptions will not affect the comparison between them.

Using these assumptions and the time required for a single correction for each code, given earlier to be $m(2w + 4)$, then the total time required for the case of two inner [[7,1,3]] codes is given by,

$$32L^3(m_2(2w_2 + 4)) + \\ 16L^3(m_1(2w_1 + 4)) + 8L^3(m_0(2w_0 + 4)) \quad (14)$$

where $w_0 = w_1 = 1$ for two inner [[7,1,3]] codes and w_2 is associated with the outer code. m_0, m_1 and m_2 are the optimal number of syndrome measurements for each code, which are identical to the single level codes analyzed earlier.

Comparing figs. 7 and 8 it is clear that if the implementation complexities for both a single inner [[23,1,7]] Golay code or a dual [[7,1,3]] Hamming code are the same, it is a more resource efficient option to make use of the [[23,1,7]] code. This was expected from [6], but now it is

clearer which code to use as the outer code for various values of L .

For $200 < L < 900$ either the $[[31,11,5]]$ or $[[63,39,5]]$ BCH codes are optimal. For $900 < L < 3000$ the $[[63,27,7]]$ BCH code becomes optimal since at this stage the two previous codes cannot achieve the required precision for these values of L . Finally for $3000 < L < 10000$ the $[[43,5,7]]$ QR code becomes optimal.

Comparing K^{0Q0} for a single layer of QEC to what is required using concatenation, you can see that for $L = 500$ there is negligible difference between the required resources needed for a single $[[127,43,13]]$ BCH code or a concatenated ($[[23,1,7]], [[31,11,5]]$) code. Hence, using concatenated correction with smaller codes requires comparable resources to a single large encoding and allows for a reduction in component precision from 10^5 to 10^4 .

The final case we wish to examine is the testing of a large scale quantum code such as Shor on a prototype quantum device. In this case we are assuming that a large number of calls can be made to the QPF subroutine in order to obtain a probability spectrum of possible results. We can therefore assume that the component precision does not need to scale as $1=n_p$, but can scale according to the results presented in section III. For this analysis we will assume that a linear scaling of $L=n_p$. All qubit and time approximations are

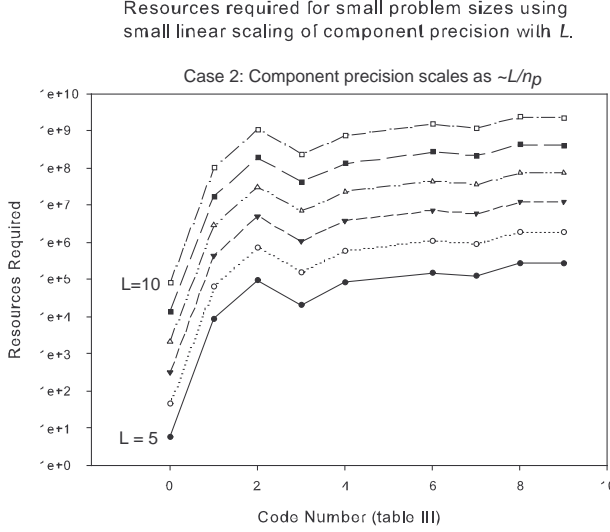


FIG. 9: Plot showing the resources needed $K^{0Q0} \sim 10^7$ for factoring small L -bit numbers. This plot assumes that we can take the component precision to scale as $L=n_p$. Since the number of circuit iterations increases quickly, the resources needed for a successful run quickly become impractical except for small L and code number.

the same as with fig. 6, but now we need to take into account that if we utilize the precision scaling of section III, the QPF subroutine is behaving slightly better than a random search and a minimum of 2^{2L} queries to the QPF subroutine is

required.

Fig. 9 only shows the results for $L = 5$ to $L = 10$ since for higher values of L , the total number of subroutine iterations become enormous. Even though utilizing this precision scaling is clearly impractical for high L in the short term this scaling could prove to be useful.

Fig. 6 shows that not using QEC only allows for running the QPF circuit for $L = 5$ bit numbers. Fig. 9 shows that utilizing a component precision scaling of $L=n_p$ allows up to $L = 10$ bit numbers to be run, without a need for QEC. Hence, if an un-encoded QPF circuit for $L = 5$ to $L = 10$ are quick, a probability spectrum for j can be obtained without the additional complications of QEC protocols. This would allow for a convenient method for testing an extremely complicated quantum circuit without the burden of also designing and implementing QEC.

V. CONCLUSION

The quantum period finding subroutine (QPF) is the essential component within Shor's factoring algorithm. Detailed simulations have shown that the complexity of the quantum circuit required to implement the QPF subroutine leads to a robustness above the naive $1=n_p$ approximation for component precision. Evidence for polynomial scaling of component precision has been demonstrated showing that the complicated topology of the quantum circuit is an important factor to stability.

Although the QPF subroutine is extremely sensitive to discrete errors, it can still perform better than a random classical search when component precision is lower than $1=n_p$. This is extremely important when it comes to testing such complex algorithms on prototype quantum computers. The additional polynomial scaling of component precision may not be practical for large problem sizes, however for smaller circuits this will prove to be beneficial.

The restriction of linear nearest neighbor designs does not significantly alter the sensitivity of the subroutine provided that appropriate LNN circuits can be designed roughly equivalent in depth and qubit numbers as non-LNN circuits.

Finally it was shown that for low values of L , the slight scaling of circuit stability with L can allow for successful factorization with no need for QEC. As L increases beyond these somewhat trivial problems, single level QEC is required with various codes becoming optimal in resources as L increases. For larger values of L single level QEC can still be used, provided that component precision is high (i.e. $< 10^5$). However, if the precision is lower ($< 10^4$) then with a moderate increase in the required resources successful factorization of large numbers $L < 10000$ is possible using concatenated correction.

Further work includes performing a detailed density matrix simulations in order to determine an exact analytical form for $P(L)$ using an appropriate simulator such as QuIDDPro [1].

VI. ACKNOWLEDGEMENTS

The authors thank A.Greentree and F. Wilhelm for discussions and comments on the manuscript. LCLH thanks the

von Delft group at LMU for their hospitality and, for financial support, the DFG through the SFB631 and the Alexander von Humboldt Foundation. This work was supported by the Australian Research Council, US National Security Agency (NSA), Advanced Research and Development Activity (ARDA) and Army Research Office (ARO) under contract number W911NF-04-1-0290.

[1] G.F. Viamontes, I.L. Markov, J.P. Hayes. *quant-ph/040311*, 2004.

[2] P.W. Shor *Society for Industrial and Applied Mathematics*, 26:1484, 1997.

[3] E. Knill, R. Laflamme, G. Milburn. *Nature*, 409:46, 2001.

[4] I.L. Chuang, R. Laflamme, P.W. Shor, W.H. Zurek. *Science*, 270:1633, 1995.

[5] C. Miquel, J.P. Paz, R. Parazzo *Phys. Rev. A*, 54:2605.

[6] A.M. Steane *Phys. Rev. A*, 60:042322, 2003.

[7] A.M. Steane *quant-ph/0202036*, 2002.

[8] M. Nielsen and I.L. Chuang. *Quantum Computation and Information*. Cambridge, Second edition, 2000.

[9] ARPA. Quantum information science and technology roadmap project. <http://qist.lanl.gov>, 2004.

[10] A. M. Steane. Error correcting codes in quantum theory. *Phys. Rev. Lett.*, 77:793, 1996.

[11] H. Imai J. Niwa, K. Matsumoto. Simulations of Quantum Error-correction Schemes. *quant-ph/0402196*, 2002.

[12] A.Fowler and L.C.L Hollenberg. *Phys. Rev. A*. 70:032329, 2004.

[13] X. Hu F. Nori L.F. Wei, X. Li. *quant-ph/0305039*, 2003.

[14] E. Knill, R. Laflamme, H.N. Barnum, D.A. Dalvit, J.J. Dziarmaga, J.E. Gubernatis, L. Guruits, G. Ortiz, and W.H. Zurek. *Los Alamos Science*, 27:38, 2002.

[15] C. Lavor, L.R.U. Manssur, and R.Portugal. *quant-ph/0303175*, 2003.

[16] V. Vedral, A. Barenco, and A. Ekert. *Phys. Rev. A*, 54:147, 1996.

[17] P. Gossett. *quant-ph/9808061*, 1998.

[18] Stephane Beauregard. *Quantum Information and Computation*, 3:175, 2003.

[19] D.Braun. *quant-ph/0110037*, 2001.

[20] C.Zalka. *quant-ph/9806084*, 1998.

[21] A.Fowler, S.J Devitt, and L.C.L Hollenberg. *Quantum Information and Computation*, 4:237, 2004.

[22] Y. Makhlin. *Quantum Information Processing*, 1:243, 2002.

[23] J.I. Cirac B. Kraus. *Phys. Rev. A*, 63:062309, 2001.

[24] S. Sastry K.B. Whaley J. Zhang, J. Vala. *Phys. Rev. A*, 67:042313, 2003.

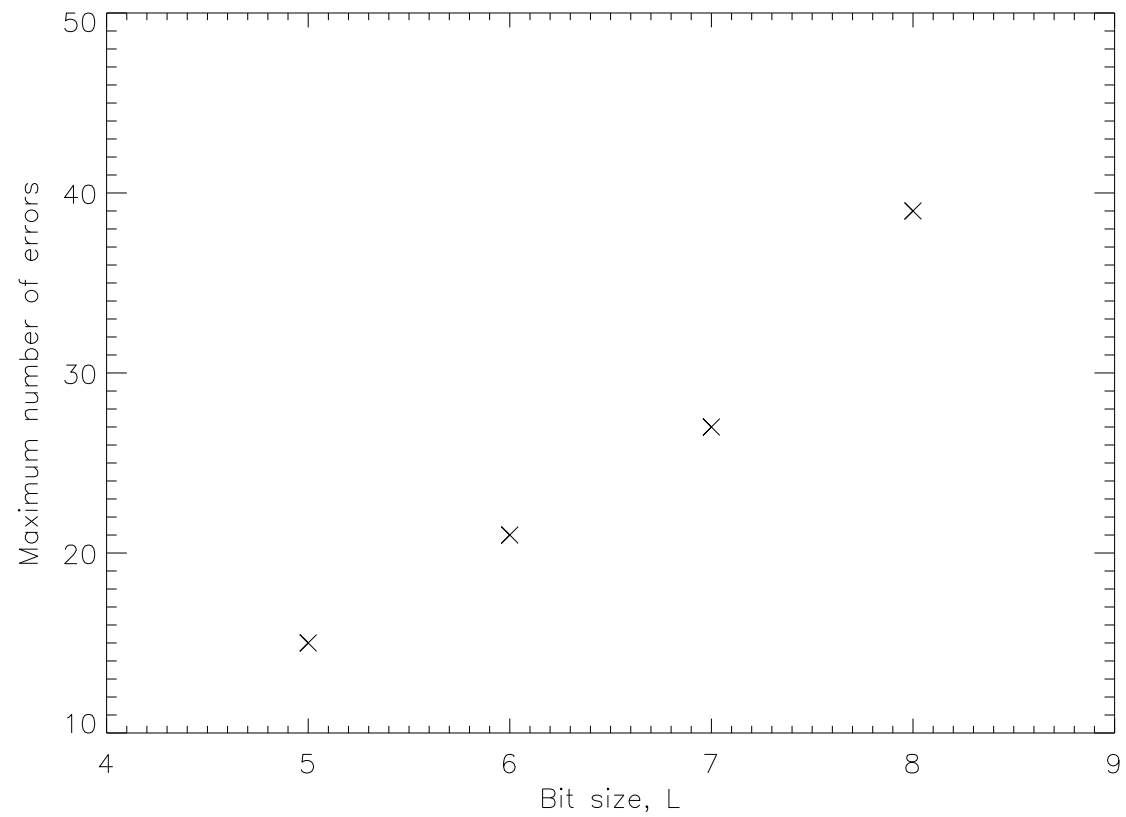
[25] A. Fowler, L.C.L. Hollenberg, and C.D Hill. *Phys. Rev. A*, 69:042314, 2004.

[26] A. Fowler. *quant-ph/0411206*, 2004.

[27] J. Cole, S.G. Schirmer, A. Greentree, C. Wellard, D.K.L. Oi, L.C.L. Hollenberg. *Phys. Rev. A*, 71:062312, 2005.

[28] A.M. Steane *Phys. Rev. A*, 54:4741, 1996.

Maximum number of errors producing non-random output as a function of L.



Maximum number of errors producing non-random output as a function of L .

